Assessment of Simplified Methods for Quantification of ^{18}F-FDHT Uptake in Patients with Metastatic Castration-Resistant Prostate Cancer

Gerbrand M. Kramer[1], Maqsood Yaqub[1], Herbert A. Vargas[2], Robert C. Schuit[1], Albert D. Windhorst[1], Alfonsus J.M. van den Eertwegh[3], Astrid A.M. van der Veldt[4,5], Andries M. Bergman[4], Eva M. Burnazi[2], Jason S. Lewis[2,6], Sua Chua[7], Kevin D. Staton[2], Brad J. Beattie[8], John L. Humm[8], Ian D. Davis[9], Andrew J. Weickhardt[10], Andrew M. Scott[10,11], Michael J. Morris[12,13], Otto S. Hoekstra[1], and Adriaan A. Lammertsma[1]

[1]Department of Radiology and Nuclear Medicine, Amsterdam UMC, Vrije Universiteit Amsterdam, Amsterdam, The Netherlands; [2]Department of Radiology, Memorial Sloan Kettering Cancer Center, New York, New York; [3]Department of Medical Oncology, Amsterdam UMC, Vrije Universiteit Amsterdam, Amsterdam, The Netherlands; [4]Department of Medical Oncology, Netherlands Cancer Institute, Amsterdam, The Netherlands; [5]Departments of Medical Oncology, Radiology, and Nuclear Medicine, Erasmus Medical Center, Rotterdam, The Netherlands; [6]Department of Radiology, Weill Cornell Medicine, New York, New York; [7]Department of Nuclear Medicine, Royal Marsden NHS Foundation Trust, Sutton, United Kingdom; [8]Department of Medical Physics, Memorial Sloan Kettering Cancer Center, New York, New York; [9]Monash University and Eastern Health, Eastern Health Clinical School, Box Hill, Australia; [10]Department of Medical Oncology, Olivia Newton-John Cancer Research Institute, Austin Hospital, Melbourne, Victoria, Australia; [11]Department of Molecular Imaging and Therapy, University of Melbourne, Heidelberg, Victoria, Australia; [12]Department of Medicine, Memorial Sloan Kettering Cancer Center, New York, New York; and [13]Department of Medicine, Weill Cornell Medicine, New York, New York

^{18}F-fluorodihydrotestosterone (^{18}F-FDHT) PET/CT potentially provides a noninvasive method for assessment of androgen receptor expression in patients with metastatic castration-resistant prostate cancer (mCRPC). The objective of this study was to assess simplified methods for quantifying ^{18}F-FDHT uptake in mCRPC patients and to assess effects of tumor perfusion on these ^{18}F-FDHT uptake metrics. **Methods:** Seventeen mCRPC patients were included in this prospective observational multicenter study. Test and retest 30-min dynamic ^{18}F-FDHT PET/CT scans with venous blood sampling were performed in 14 patients. In addition, arterial blood sampling and dynamic ^{15}O-H_2O scans were obtained in a subset of 6 patients. Several simplified methods were assessed: Patlak plots; SUV normalized to body weight (SUV_{BW}), lean body mass (SUV_{LBM}), whole blood (SUV_{WB}), parent plasma activity concentration (SUV_{PP}), area under the parent plasma curve ($SUV_{AUC,PP}$), and area under the whole-blood input curve ($SUV_{AUC,WB}$); and SUV_{BW} corrected for sex hormone–binding globulin levels (SUV_{SHBG}). Results were correlated with parameters derived from full pharmacokinetic ^{18}F-FDHT and ^{15}O-H_2O. Finally, the repeatability of individual quantitative uptake metrics was assessed. **Results:** Eighty-seven ^{18}F-FDHT–avid lesions were evaluated. ^{18}F-FDHT uptake was best described by an irreversible 2-tissue-compartment model. Replacing the continuous metabolite-corrected arterial plasma input function with an image-derived input function in combination with venous sample data provided similar K_i results ($R^2 = 0.98$). Patlak K_i and $SUV_{AUC,PP}$ showed an excellent correlation ($R^2 > 0.9$). SUV_{BW} showed a moderate correlation to K_i ($R^2 = 0.70$, presumably due to fast ^{18}F-FDHT metabolism. When calculating SUV_{SHBG}, correlation to K_i improved ($R^2 = 0.88$). The repeatability of full kinetic modeling parameters was inferior to that of simplified methods (repeatability coefficients $> 36\%$ vs. $< 28\%$, respectively). ^{18}F-FDHT uptake showed minimal blood flow dependency. **Conclusion:** ^{18}F-FDHT kinetics in mCRPC patients are best described by an irreversible 2-tissue-compartment model with blood volume parameter. $SUV_{AUC,PP}$ showed a near-perfect correlation with the irreversible 2-tissue-compartment model analysis and can be used for accurate quantification of ^{18}F-FDHT uptake in whole-body PET/CT scans. In addition, SUV_{SHBG} could potentially be used as an even simpler method to quantify ^{18}F-FDHT uptake when less complex scanning protocols and accuracy are required.

Key Words: FDHT; PET/CT; prostate cancer; quantification

J Nucl Med 2019; 60:1221–1227
DOI: 10.2967/jnumed.118.220111

Prostate cancer is the most frequently diagnosed form of cancer in developed parts of the world and the second most common cause of cancer-related mortality in U.S. men, leading to about 29,000 annual deaths (*1,2*). The androgen receptor (AR) plays a central role in both early and later stages of prostate cancer, including metastatic castration-resistant prostate cancer (mCRPC). For mCRPC, several mechanisms of AR-signaling persistence have been proposed, including persisting androgen production, AR overexpression, AR-splice variation, and AR transcription via alternative signaling pathways (*3*). Several agents have been developed that specifically target the AR (e.g., enzalutamide and abiraterone). In mCRPC patients, both with and without prior treatment with docetaxel, these drugs have been shown to result in improved survival and quality of life (*4,5*).

^{18}F-fluorodihydrotestosterone (^{18}F-FDHT) is a positron-emitting tracer that provides a means to image the AR in vivo in mCRPC

Received Sep. 7, 2018; revision accepted Feb. 6, 2019.
For correspondence or reprints contact: Gerbrand M. Kramer, Department of Radiology and Nuclear Medicine, Amsterdam UMC, Vrije Universiteit Amsterdam, P.O. Box 7057, 1007 MB Amsterdam, the Netherlands.
E-mail: ge.kramer@vumc.nl
Published online Mar. 8, 2019.

patients (*6,7*). Therefore, ^{18}F-FDHT PET/CT could potentially be used as an imaging biomarker to evaluate AR status and pharmacologic targeting on a lesion-by-lesion level. This potential is of particular significance because mechanisms of persistent AR signaling can differ between metastatic lesions (*8,9*). In mCRPC, direct assessment of AR using ^{18}F-FDHT might aid AR-targeted drug development, and more personalized treatment planning, thereby potentially preventing unnecessary toxicities and costs.

Accurate quantification is required for objective evaluation of ^{18}F-FDHT uptake in mCRPC lesions. The gold standard for quantification of tracer uptake is pharmacokinetic modeling using nonlinear regression (NLR) in combination with a metabolite-corrected arterial plasma input function (*10*). At present, NLR is incompatible with the whole-body acquisitions typically required in patients with metastatic disease. Development of total-body PET scanners may overcome this problem. Moreover, because of its complexity, this method it is not well suited for daily clinical practice or large multicenter studies, in which simpler methods such as SUVs are preferred. Although pharmacokinetic assessment of ^{18}F-FDHT uptake has been performed by Beattie et al. (*6*), a population-based input function was used rather than individually measured arterial input functions. This method could have confounded results because of intersubject differences in individual arterial input function.

Full understanding of ^{18}F-FDHT kinetics is essential for developing simplified methods to quantify ^{18}F-FDHT uptake in clinical practice. Therefore, the objectives of this study were, first, to identify the optimal pharmacokinetic model for quantifying ^{18}F-FDHT kinetics in mCRPC patients using individually measured arterial input function; second, to comprehensively investigate whether simplified methods can be used for accurate quantification of ^{18}F-FDHT uptake; third, to measure the repeatability of ^{18}F-FDHT uptake metrics; and fourth, to assess potentially confounding effects of perfusion on these simplified ^{18}F-FDHT uptake metrics.

MATERIALS AND METHODS

Patients

Between July 2014 and October 2017, 17 histologically proven mCRPC patients were included at the VU University Medical Center and at Memorial Sloan Kettering Cancer Center. Fifteen patients were also included in a previous publication assessing the repeatability of whole-body quantitative ^{18}F-FDHT uptake metrics (*11*). Patient eligibility criteria were castration-resistant prostate cancer (castrate levels of serum testosterone < 1.7 nmol·L^{-1} [50 ng·dL^{-1}]), no treatment with enzalutamide or other antiandrogens within 4 wk before study entry, no other malignancies, at least 1 lesion within the field of view positioned over the ascending aorta, and progressive disease based on any of the following: a rise in serum PSA through 3 consecutive measurements, RECIST 1.1 imaging evidence of progressive disease, or a bone scan showing at least 2 new metastatic lesions not attributable to the flare phenomenon. Patients without orchiectomy remained on androgen depletion therapy with a gonadotropin-releasing hormone analog or inhibitor during the study. This study was approved by the institutional review boards of both centers, and all participants gave written informed consent before study enrollment. This trial is registered at clinicaltrials.gov (NCT00588185; this number applies only to Memorial Sloan Kettering, the only United States–based site).

PET Imaging

^{18}F-FDHT PET/CT scans were obtained using a GE Healthcare 690 or 710 or a Philips Gemini TF 64 PET/CT scanner. All participants underwent double baseline ^{18}F-FDHT scans on 2 consecutive days. Sex hormone–binding globulin levels were determined on the day of the first scan. First, a low-dose CT scan (120–140 kV) was performed during tidal breathing, directly followed by a 30-min dynamic ^{18}F-FDHT PET scan over the thorax starting simultaneously with intravenous ^{18}F-FDHT administration. The tracer was administered either manually at a rate of 0.5 mL·s^{-1} during 3–10 s followed by more than 40 mL of saline in 30–60 s, or using an automated injector (Medrad) flushed with 40 mL of saline (5 mL at 0.8 mL·s^{-1} followed by 35 mL at 2 mL·s^{-1}). After injection, residual activity in the syringe and lines was measured. Dynamic ^{18}F-FDHT data were reconstructed into 19 frames (6×5, 3×10, 4×60, 2×150, and 4×300 s) and corrected for detector inhomogeneity, dead time, decay, scatter, random coincidences, and photon attenuation, the last of these using the low-dose CT scan. Ordered-subset expectation maximization was used for reconstruction of the images. In addition, during the dynamic ^{18}F-FDHT scan, 3 manual venous samples were drawn from a separate intravenous cannula at 5, 10, and 30 min after injection (*12*). For all samples, whole-blood and plasma activity concentrations were measured, as well as parent and metabolite fractions of ^{18}F-FDHT. Radiometabolite analysis was performed using high-performance liquid chromatography at the VU University Medical Center. At Memorial Sloan Kettering Cancer Center, a simplified method was used. High-performance liquid chromatography was performed for only the first and last blood samples; for the other samples, an extraction technique was used, and combined with the high-performance liquid chromatography data, the parent fraction was determined. Details on the radiometabolite analysis method used can be found in a previous publication by Beattie et al. (*6*).

Furthermore, a subset of patients underwent continuous arterial sampling at 5 mL·min^{-1} during the first 5 min and at 2.5 mL·min^{-1} thereafter until the end of the dynamic ^{18}F-FDHT scan. Continuous sampling was interrupted at 5, 10, 15, 20, 30, and 45 min after injection to obtain manual arterial samples for determination of whole-blood activity concentrations, plasma activity concentrations, and parent and metabolite fractions. These patients also underwent a dynamic 10-min ^{15}O-H_2O scan before the first dynamic ^{18}F-FDHT scan. ^{15}O-H_2O (370 MBq) was administered using an automated injector (Medrad) and flushed using 40 mL of saline (5 mL at 0.8 mL·s^{-1} followed by 35 mL at 2 mL·s^{-1}). After the ^{15}O-H_2O PET scan, a low-dose CT scan (120 kV) was acquired for attenuation correction. The dynamic ^{15}O-H_2O data were reconstructed into 26 frames (1×10, 8×5, 4×10, 2×15, 3×20, 2×30, and 6×60 s) using the same correction and reconstruction methods as for the dynamic ^{18}F-FDHT scans.

Data Analysis

All ^{18}F-FDHT–avid tumors were delineated on an averaged image generated from the last 15 min of the dynamic ^{18}F-FDHT scan, using a 50% isocontour of SUV_{peak} (sphere of 1.2-cm diameter, positioned to maximize its mean value) corrected for local background to obtain volumes of interest (Fig. 1) (*12*). Time–activity curves were produced by projecting tumor volumes of interest on the dynamic ^{18}F-FDHT and, when applicable, ^{15}O-H_2O scans. In addition, image-derived input functions (IDIFs) were obtained from ^{18}F-FDHT and ^{15}O-H_2O

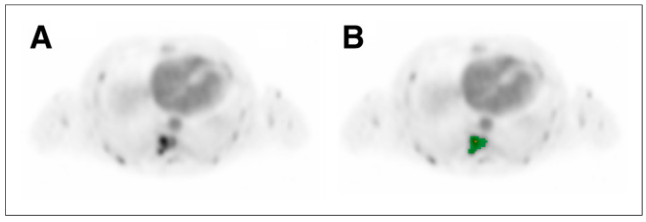

FIGURE 1. (A) Example of averaged image generated from last 15 min of dynamic ^{18}F-FDHT scan. (B) All tumors were delineated using 50% isocontour of SUV_{peak} (sphere of 1.2-cm diameter, positioned to maximize its mean value) corrected for local background. Yellow voxel indicates hottest voxel in volume of interest.

scans by placing a 2 × 2 voxel volume of interest centrally on the ascending aorta in 5 consecutive planes using an early frame in which the blood pool was clearly visible. Corresponding time–activity curves were generated by projecting these volumes of interest onto ^{18}F-FDHT and ^{15}O-H_2O scans.

Both arterially sampled input curves and IDIFs (600–2,000 s) were calibrated using the manual arterial blood samples. Subsequently, these calibrated input curves were corrected for plasma–to–whole-blood ratios and metabolites to generate parent plasma input functions using a multiexponential fit and Hill fit (*13*), respectively. For IDIFs, this procedure was repeated using the manual venous blood samples ($IDIF_{venous}$).

Pharmacokinetic modeling was performed using in-house–developed software in MATLAB (MathWorks Inc.). ^{15}O-H_2O scans were analyzed using the standard single-tissue reversible arterial input model with an additional blood volume fraction parameter, and the kinetic rate constant K_1 was used as the outcome parameter (*14*). ^{18}F-FDHT data were analyzed using 1-tissue and both irreversible and reversible 2-tissue-compartment models, all with an additional blood volume fraction parameter consisting of whole-blood activity (*10,15*). Net influx rate (K_i) and volume of distribution (V_T) were calculated from fitted kinetic rate constants: 2-tissue irreversible $K_i = K_1 \cdot k_3/(k_2 + k_3)$, 2-tissue reversible 2-compartment $V_T = K_1/k_2 \cdot (1 + k_3/k_4)$, and 2-tissue reversible 1-compartment $V_T = K_1/k_2$. The optimal fit was obtained from the best among 20 constrained fits, each initialized with randomly chosen starting parameters. The constraints of the pharmacokinetic parameters were 0–2 for K_1, 0–100 for k_2, 0.025–100 for k_3, and 0–100 for k_3/k_4. Furthermore, several simplified uptake metrics were derived from the ^{18}F-FDHT data: Patlak K_i (t* = 5 min after injection); SUV normalized to body weight (SUV_{BW}), lean body mass (SUV_{LBM}), whole-blood activity concentration (SUV_{WB}), parent plasma concentration (SUV_{PP}), area under the whole-blood input curve ($SUV_{AUC,WB}$), and area under the parent plasma input curve ($SUV_{AUC,PP}$); and SUV_{BW} corrected for serum SHBG levels (SUV_{SHBG} = SUV_{BW}/serum SHBG). All SUV uptake intervals were set to 20–30 min after injection (*6*).

TABLE 1
Patient Characteristics (n = 14)

Characteristic	Median	n
Age (y)	69 (58–85)	
Length (cm)	180 (170–194)	
Weight (kg)	83 (65–125)	
Gleason score	8 (5–10)	
P-specific antigen (ng/mL)	102.5 (0.5–1,602)	
SHBG (nmol/L)	41 (19–81)	
Injected activity (MBq)		
Test	197 (174–337)	
Retest	196 (186–342)	
Residual dose (MBq)		
Test	31.4 (18.2–55.7)	
Retest	34.5 (6.1–53.5)	
Lesions		
Bone		75
Lymph node		12
Location		
Thoracic vertebrae		36
Ribs		24
Sternum		8
Scapulae		6
Humerus		1
Mediastinal lymph nodes		12
Axillary lymph nodes		1
Scanner type		
Philips Gemini TF 64		11
GE Healthcare 690 or 710		3
Sampling		
Arterial		6
Venous		14

Data in parentheses are ranges.

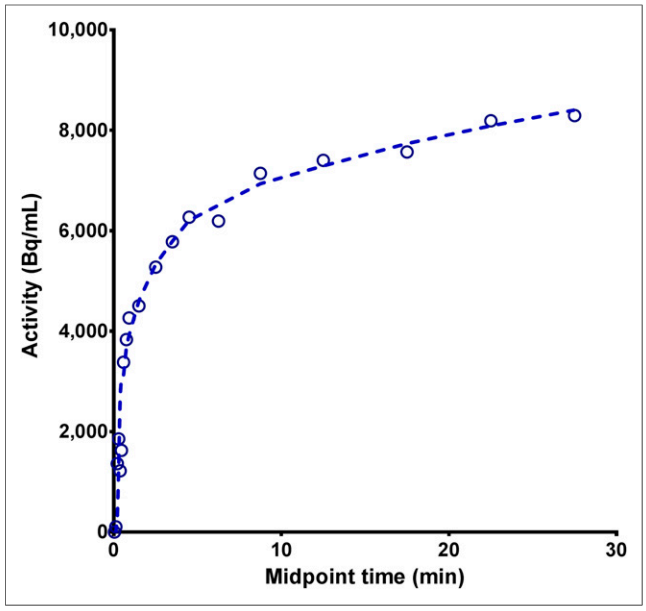

FIGURE 2. Typical example of ^{18}F-FDHT uptake in metastatic prostate cancer lesions fitted using irreversible 2-tissue model with blood volume fraction parameter.

Statistical Analysis

Normality of the data was assessed visually using a quantile–quantile plot and histogram analysis. The Akaike criterion was used to select the preferred model for describing kinetics of ^{18}F-FDHT in patients undergoing arterial blood sampling (*16*). Pharmacokinetic outcome measures calculated using the metabolite-corrected arterial plasma input functions were correlated against pharmacokinetic outcome measures obtained using IDIFs and perfusion metrics. Performance of simplified uptake metrics was assessed in a head-to-head comparison with pharmacokinetic outcome measures from NLR. These analyses were performed using linear regression analysis, intraclass correlation coefficients, and Bland–Altman plots. In addition, when applicable, the repeatability of all outcome measures was assessed using repeatability coefficients (RCs) calculated as 1.96 × SD of the relative differences per lesion. Levene testing was performed to assess differences in RCs between outcome measures. Differences were deemed significant if P was less than 0.05. All statistical analyses were performed using SPSS 22.0.

RESULTS

Pharmacokinetic Modeling

Fourteen patients, with a total of 87 lesions, were enrolled (Table 1). Three patients were excluded because of incomplete or

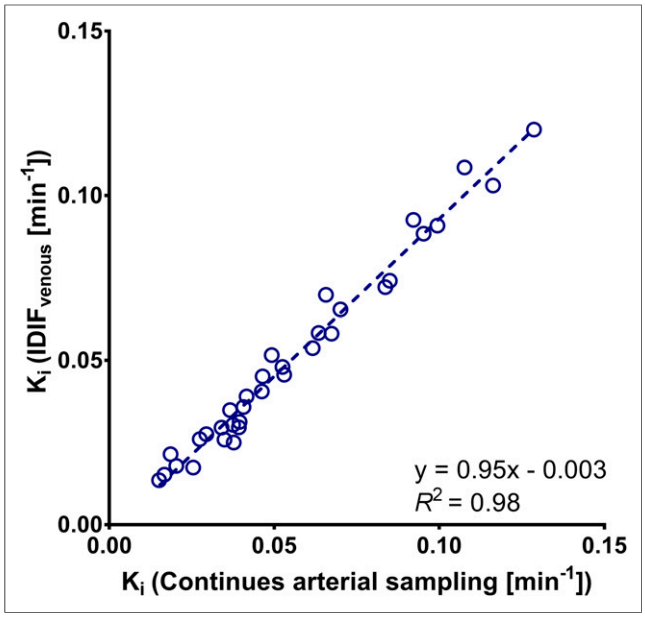

FIGURE 3. ^{18}F-FDHT K_i obtained using IDIF corrected using venous blood samples ($IDIF_{venous}$) plotted against those obtained using continuous arterial sampling (n = 34).

missing blood sample data. Overall, plasma-to-blood ratios remained stable over time; however, ^{18}F-FDHT underwent fast metabolism and about 90% was metabolized at 30 min after injection (Supplemental Fig. 1; supplemental materials are available at http://jnm.snmjournals.org).

Continuous arterial blood sampling in combination with manual arterial sampling was performed in a subset of 6 patients with 44 ^{18}F-FDHT–avid lesions. On the basis of the Akaike criterion, tumor time–activity curves were best described by an irreversible 2-tissue model in 34%, a reversible 2-tissue 2-compartment model in 27% and a reversible 2-tissue 1-compartment model in 39% of the lesions. In 52% of the lesions, the difference in Akaike criterion between the pharmacokinetic models was less than 15 points. All individual K_i values were within reference range, whereas V_T values suffered from outliers in 36% of the cases for the reversible 2-tissue 2-compartment model and 7% for the reversible 2-tissue 1-compartment model. Therefore, the irreversible 2-tissue model was used for further evaluation of ^{18}F-FDHT (Fig. 2). Replacing the continuous arterial plasma input function with $IDIF_{venous}$ provided similar K_i results (R^2 = 0.98; intraclass correlation coefficient, 0.99) (Fig. 3). The results of full kinetic modeling and simplified methods are shown in Supplemental Table 1.

Considering the strong correlation with K_i obtained using continuous arterial sampling, K_i obtained using $IDIF_{venous}$ was used for validation of simplified methods. Fourteen lesions were excluded because of unrealistically high k_2 values and SDs (k_2 > 1). An excellent correlation was found between Patlak K_i and NLR-derived K_i (R^2 = 0.99; intraclass correlation coefficient, 0.99). This was also the case for $SUV_{AUC,PP}$, but the performance of more simplified methods was poorer (Fig. 4; Table 2; Supplemental Fig. 2). No significant differences were found in accuracy between SUV_{BW} and SUV_{LBM}. When SUV_{BW} was corrected for serum SHBG levels (SUV_{SHBG}), overall correlation with full kinetic modeling improved (R^2 = 0.88). A direct comparison of serum SHBG to the rate of ^{18}F-FDHT metabolism, calculated as the AUC of the parent plasma input function, did not show a strong relationship (R^2 = 0.32). All simplified methods reached equilibrium at 30 min after injection, except for SUV_{pp}, which still showed a steep increase.

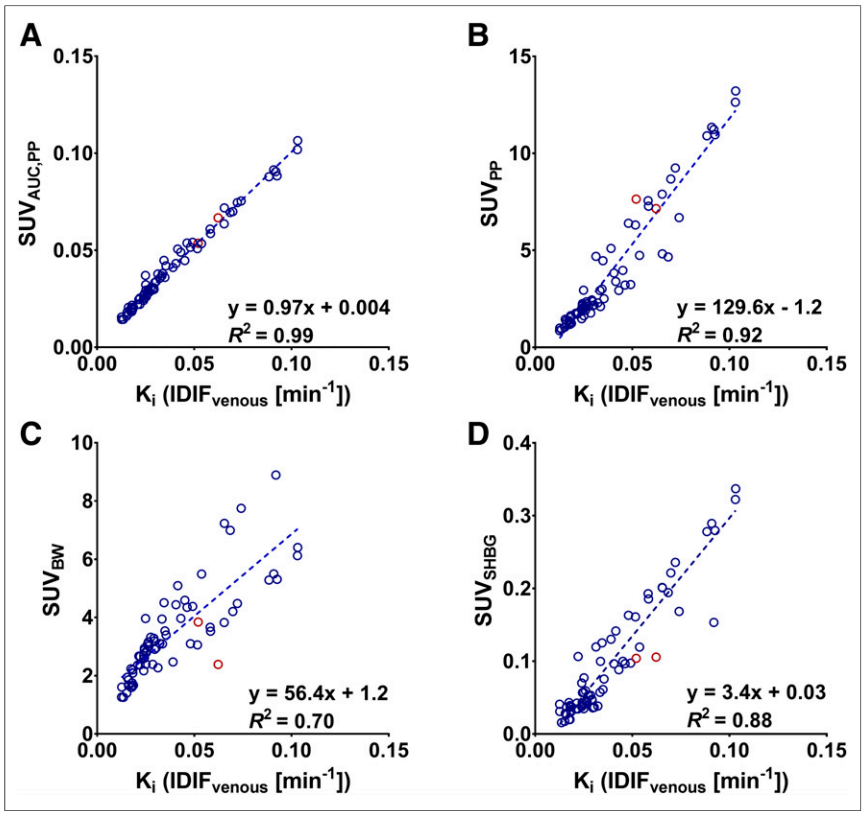

FIGURE 4. Scatterplots showing correlation of ^{18}F-FDHT $SUV_{AUC,PP}$ (A), SUV_{PP} (B), SUV_{BW} (C), and SUV_{SHBG} (D) with K_i obtained using IDIF corrected for metabolites using venous blood samples ($IDIF_{venous}$) (n = 87). Blue = Philips Gemini TF 64; red = GE Healthcare 690 or 710.

Repeatability

Repeated baseline scans were available in 10 patients with a total of 80 lesions. Median plasma-to-blood and parent plasma fractions at 30 min were not significantly different between test and retest scans (P > 0.7) (Supplemental Fig. 1). The correlation between test and retest scans was strong for all quantitative metrics (R^2 = 0.86–0.93; intraclass correlation coefficient, >0.95). The RC of NLR-derived K_i using IDIF corrected with venous sample data was 36% (Fig. 5). Except for SUV_{pp}, quantitatively assessing ^{18}F-FDHT uptake using simplified methods reduced variability (RC, 23%–31%) (Table 3; Fig. 5; Supplemental Table 2; Supplemental Fig. 3). The repeatability of all uptake metrics showed a trend toward dependency on lesion size. In addition, for SUV_{pp} and SUV_{BW}, repeatability appeared to improve for higher SUVs.

TABLE 2
Correlation of Simplified Methods with K_i Obtained Using Pharmacokinetic Modeling

Method	Continuous arterial sampling			$IDIF_{venous}$		
	R^2	Slope	Intercept	R^2	Slope	Intercept
Patlak K_i	0.99	0.90	0.00	0.99	0.93	0.00
$SUV_{AUC,PP}$	0.99	0.94	0.00	0.99	0.97	0.00
$SUV_{AUC,WB}$	0.83	0.41	0.01	0.83	0.45	0.00
SUV_{PP}	0.96	116.99	−0.46	0.92	129.57	−1.16
SUV_{WB}	0.77	10.88	0.24	0.77	11.69	0.29
SUV_{BW}	0.76	55.91	0.81	0.70	56.40	1.23
SUV_{LBM}	0.73	41.64	0.75	0.70	40.97	1.06
SUV_{SHBG}	0.80	2.88	−0.30	0.88	3.19	−0.03

$IDIF_{venous}$ = NLR using IDIF corrected using venous blood samples.

Perfusion

Thirty-five lesions (30 bone and 5 lymph node metastases) were available for assessing the correlation between perfusion and quantitative ^{18}F-FDHT uptake metrics. K_i values obtained using the irreversible 2-tissue-compartment model with $IDIF_{venous}$ as well as ^{18}F-FDHT plasma extraction showed minimal blood flow dependency (R_2 = 0.23 and 0.30, respectively) (Fig. 6). In addition, the effects of perfusion on the discrepancy between SUV- and NLR-based K_i for ^{18}F-FDHT were assessed by plotting the ratio of SUV/K_i against ^{15}O-H_2O–derived K_1. This plot showed no correlation with blood flow for any of the SUVs ($R^2 \leq 0.01$) (Supplemental Fig. 4).

DISCUSSION

This multicenter study addressed the important clinical question of whether simplified uptake metrics can be used to measure ^{18}F-FDHT uptake in mCRPC both accurately and precisely. An irreversible 2-tissue model with blood volume fraction parameter was preferred for characterizing tumor ^{18}F-FDHT kinetics. This is congruent with previous findings from Beattie et al. (*6*), for whom both irreversible 1- and 2-tissue models provided the best fits in most cases. The preference for the irreversible 2-tissue model is also logical from a physiologic perspective. In this model, K_1 presumably represents influx of ^{18}F-FDHT into the cell. After influx, ^{18}F-FDHT binds to AR (the presumptive second compartment described by k_3) and is then transported into the nucleus. It could therefore be argued that k_3 is a more appropriate measure for assessment of AR expression, as it describes the binding of ^{18}F-FDHT to the AR rather than uptake in the prostate cancer cell. Finally, k_2 represents efflux of unbound ^{18}F-FDHT out of the prostate cancer cell. It has been suggested that ^{18}F-FDHT binding might be reversible at later time points (*6,17*) and that slow reversibility may potentially develop more than 1 h after injection of ^{18}F-FDHT.

Pharmacokinetic measures obtained using an $IDIF_{venous}$ correlated well with those obtained using a continuous arterial plasma input function. There was a slight negative bias (5%), which could be due to temporal differences between the 2 input functions. In addition, no significant differences were found between plasma-to-blood ratios and parent fractions of venous and arterial blood samples. This indicates that arterial blood sampling is not required in the case of ^{18}F-FDHT quantification. There was an almost perfect correlation between $SUV_{AUC,PP}$ and K_i derived from pharmacokinetic analysis, eliminating the need for dynamic scanning. Nevertheless, $SUV_{AUC,PP}$ still requires an additional 30-min static PET scan over the chest together with metabolite analysis of several venous blood samples. This enables accurate quantification of lesions outside the thorax, although metabolite analysis may limit its feasibility in multicenter studies and daily clinical practice. Automation of ^{18}F-FDHT metabolite analysis could potentially overcome these limitations.

As an alternative, SUV requires only a single static whole-body scan without any blood sampling. However, in line with Beattie et al. (*6*), SUV showed only a moderate correlation with pharmacokinetic outcome measures. This poorer correlation was primarily caused by 1 subject with very extensive disease (>40 lesions) and relatively low SHBG levels. In blood, most dihydrotestosterone is bound to proteins (mainly SHBG). Yet, as postulated in the free hormone hypothesis, only free circulating dihydrotestosterone is able to bind to the AR (*18,19*). In a murine prostate cancer model, Larimer et al. (*17*) showed that differences in tissue-to-blood ratios between free circulating and SHBG-bound ^{18}F-FDHT were small at 1 h after injection. However, blood-pool activity was significantly higher in SHBG-bound ^{18}F-FDHT at 1 h after injection, indicating a decreased

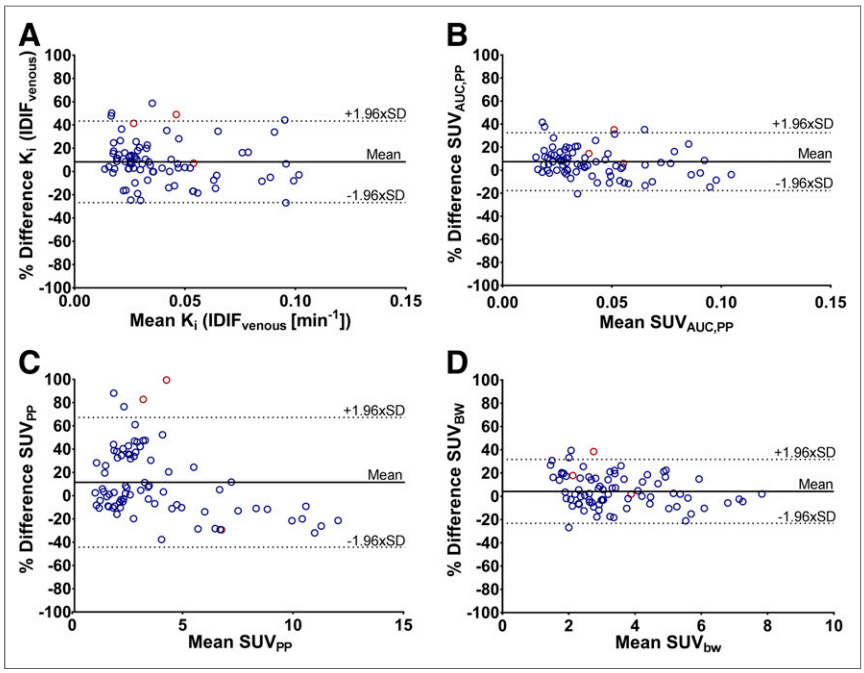

FIGURE 5. Bland–Altman plots showing relative differences in ^{18}F-FDHT uptake between test and retest K_i obtained using IDIF corrected using venous blood samples (A), $SUV_{AUC,PP}$ (B), SUV_{PP} (C), and SUV_{BW} (D) (n = 80). Blue = Philips Gemini TF 64; red = GE 690 or GE710.

TABLE 3
RCs of Several Quantitative ^{18}F-FDHT Quantitative Uptake Metrics per Lesion

Metric	Absolute difference		Relative difference	
	Mean	RC	Mean (%)	RC (%)
$IDIF_{venous}$ K_i	0.003	0.037	8.3	35.0
Patlak K_i	0.003	0.034	8.2	31.3
$SUV_{AUC,PP}$	0.003	0.038	7.4	25.1
$SUV_{AUC,WB}$	0.002	0.023	3.1	23.7
SUV_{PP}	0.089	4.178	11.4	55.8
SUV_{WB}	0.062	0.660	2.4	25.1
SUV_{BW}	0.277	2.878	4.2	27.1
SUV_{LBM}	0.230	2.239	4.3	27.1

$IDIF_{venous}$ = NLR using IDIF corrected using venous blood samples.

metabolic rate compared with freely circulating FDHT and an increased tumor uptake, as tissue-to-blood ratios are comparable. Normalizing SUV for interpatient differences in serum SHBG levels significantly improved correlation with NLR-derived K_i. Nevertheless, the rate of ^{18}F-FDHT metabolism levels only showed a moderate correlation with serum SHBG (data not shown). Determining serum SHBG just before the ^{18}F-FDHT scan could potentially be used as a surrogate for more cumbersome parent plasma fraction measurements. SHBG measurements are widely available, which would facilitate application in clinical practice or larger trials. However, further research is needed before SHBG can be used as a surrogate for metabolite analysis.

Changes in tumor perfusion due to physiologic variability or treatment could potentially affect tracer uptake when it is perfusion-limited. For K_i, a poor correlation was found with ^{15}O-H_2O–derived K_1, and therefore K_i does not seem to depend on tumor perfusion. Even though ^{18}F-FDHT is rapidly cleared from blood plasma, k_3 values were relatively small compared with k_2 values, thereby limiting the effects of perfusion on ^{18}F-FDHT uptake. SUV_{BW} and SUV_{SHBG} showed somewhat stronger and weaker correlations with ^{15}O-H_2O K_1, respectively. However, discrepancies of SUV_{BW} and SUV_{SHBG} with ^{18}F-FDHT K_i were not due to differences in perfusion.

Before quantitative uptake metrics can be used in a response assessment setting, repeatability should be known. A highly accurate parameter cannot be used for response measurements if precision is poor. RCs found for SUV in the present study were similar to those found in a previous study for whole-body quantitative ^{18}F-FDHT uptake metrics and in line with those of other ^{18}F-labeled tracers (*11,20,21*). The repeatability of full kinetic modeling parameters obtained using an irreversible 2-tissue-compartment model showed higher variability than those of more simplified methods, with the exception of SUV_{PP}. NLR analysis is known to be more vulnerable to noise, but it can account for changes in pharmacokinetics after therapy. Pharmacokinetic assessment of quantitative tracer uptake should therefore be performed before simplified methods can be used in a response evaluation setting. In the present study, no RCs could be calculated for SUV_{SHBG} as SHBG levels were determined before only the first ^{18}F-FDHT scan. Nevertheless, previous studies found small fluctuations in SHBG levels within 2 consecutive days, and the influence of SHBG on repeatability is therefore expected to be minimal (*22*).

In the present study, validation of simplified ^{18}F-FDHT uptake metrics was performed in mCRPC patients. This is an essential step in the development of ^{18}F-FDHT as an imaging biomarker for prognosis, response, and AR-targeted drug development by direct evaluation of AR status on a lesion-by-lesion level. $SUV_{AUC,PP}$ and, to a lesser extent, SUV_{SHBG} seemed to be the preferred simplified methods for quantification of ^{18}F-FDHT uptake. SUV_{SHBG} is more attractive in clinical practice and for larger multicenter trials, as it requires only a single whole-body ^{18}F-FDHT scan and SHBG blood sample. However, the exact RCs of this uptake measure still need to be determined. The correlation of $SUV_{AUC,PP}$ with K_i derived from full pharmacokinetic analysis was much stronger than for SUV_{SHBG}, although at the cost of an additional early scan over the chest and metabolite analysis to obtain the parent plasma input function. This method is preferred when high accuracy is required. An additional advantage of including $SUV_{AUC,PP}$ in an investigational setting is that more simplified methods can also be assessed. $SUV_{AUC,PP}$ and SUV_{SHBG} can both be used for whole-body acquisitions, which is essential in mCRPC because most lesions are located outside of the thorax. As a next step in the development of ^{18}F-FDHT PET/CT as an imaging biomarker, the performance of these quantitative uptake metrics need to be assessed in biologic and clinical validation studies.

The small number of patients is an inherent limitation to pharmacokinetic modeling studies. High patient burden and costly procedures limit the number of scans that can be acquired. Nevertheless, we performed a multicenter study and double baseline scanning to maximize the reliability of the pharmacokinetic ^{18}F-FDHT modeling. Unfortunately, most scans were obtained from 1 center; however, multicenter pharmacokinetic studies are unusual, and most pharmacokinetic studies are performed in single-center setting.

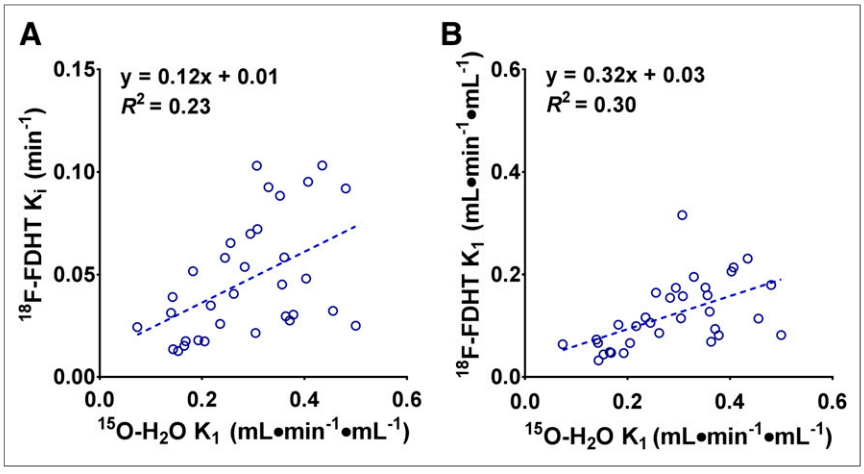

FIGURE 6. NLR-based K_i (A) and K_1 (B) using venous blood sampling and SUV_{SHBG} plotted against ^{15}O-H_2O based K_1.

CONCLUSION

An irreversible 2-tissue-compartment model with blood volume parameter best described ^{18}F-FDHT kinetics in mCRPC patients. $SUV_{AUC,PP}$ correlated nearly perfectly with K_i obtained using full pharmacokinetic analysis and can be used for accurate quantification of ^{18}F-FDHT uptake in whole-body PET/CT scans. Therefore, $SUV_{AUC,PP}$ is recommended when high accuracy is required. In addition, SUV_{SHBG} also showed a strong correlation with K_i and might be considered when less accuracy is required.

DISCLOSURE

This study was funded by a Movember Foundation Global Action Plan award. The Memorial Sloan Kettering Cancer Center is supported by NIH/NCI Cancer Center Support Grant P30 CA008748. Ian Davis is supported by an Australian NHMRC Practitioner Fellowship (APP1102604). No other potential conflict of interest relevant to this article was reported.

KEY POINTS

QUESTION: Can simplified methods be used for accurate quantification of ^{18}F-FDHT uptake in metastatic castration-resistant prostate cancer lesions?

PERTINENT FINDINGS: In this prospective observational multicenter study, we found that ^{18}F-FDHT uptake can be accurately quantified using SUV corrected for area under the venous parent plasma curve ($R^2 = 0.99$). SUV normalized to body weight shows a moderate correlation ($R^2 = 0.70$); however, correction for sex hormone–binding globulin levels improves results ($R^2 = 0.88$).

IMPLICATIONS FOR PATIENT CARE: This study is an essential step in the development of ^{18}F-FDHT PET/CT as an imaging biomarker for prognosis, response, and AR-targeted drug development by direct evaluation of AR status on a lesion-by-lesion level.

REFERENCES

1. Ferlay J, Soerjomataram I, Dikshit R, et al. Cancer incidence and mortality worldwide: sources, methods and major patterns in GLOBOCAN 2012. *Int J Cancer.* 2015;136:E359–E386.
2. Siegel RL, Miller KD, Jemal A. Cancer statistics, 2018. *CA Cancer J Clin.* 2018;68:7–30.
3. Ferraldeschi R, Welti J, Luo J, Attard G, de Bono JS. Targeting the androgen receptor pathway in castration-resistant prostate cancer: progresses and prospects. *Oncogene.* 2015;34:1745–1757.
4. Scher HI, Fizazi K, Saad F, et al. Increased survival with enzalutamide in prostate cancer after chemotherapy. *N Engl J Med.* 2012;367:1187–1197.
5. Beer TM, Armstrong AJ, Rathkopf D, et al. Enzalutamide in men with chemotherapy-naive metastatic castration-resistant prostate cancer: extended analysis of the phase 3 PREVAIL study. *Eur Urol.* 2017;71:151–154.
6. Beattie BJ, Smith-Jones PM, Jhanwar YS, et al. Pharmacokinetic assessment of the uptake of 16beta-^{18}F-fluoro-5alpha-dihydrotestosterone (FDHT) in prostate tumors as measured by PET. *J Nucl Med.* 2010;51:183–192.
7. Bonasera TA, O'Neil JP, Xu M, et al. Preclinical evaluation of fluorine-18-labeled androgen receptor ligands in baboons. *J Nucl Med.* 1996;37:1009–1015.
8. Larson SM, Morris M, Gunther I, et al. Tumor localization of 16beta-^{18}F-fluoro-5alpha-dihydrotestosterone versus ^{18}F-FDG in patients with progressive, metastatic prostate cancer. *J Nucl Med.* 2004;45:366–373.
9. Vargas HA, Wassberg C, Fox JJ, et al. Bone metastases in castration-resistant prostate cancer: associations between morphologic CT patterns, glycolytic activity, and androgen receptor expression on PET and overall survival. *Radiology.* 2014;271:220–229.
10. Gunn RN, Gunn SR, Cunningham VJ. Positron emission tomography compartmental models. *J Cereb Blood Flow Metab.* 2001;21:635–652.
11. Vargas HA, Kramer GM, Scott AM, et al. Reproducibility and repeatability of semiquantitative ^{18}F-fluorodihydrotestosterone uptake metrics in castration-resistant prostate cancer metastases: a prospective multicenter study. *J Nucl Med.* 2018;59:1516–1523.
12. Frings V, Yaqub M, Hoyng LL, et al. Assessment of simplified methods to measure ^{18}F-FLT uptake changes in EGFR-mutated non-small cell lung cancer patients undergoing EGFR tyrosine kinase inhibitor treatment. *J Nucl Med.* 2014;55:1417–1423.
13. Gunn RN, Sargent PA, Bench CJ, et al. Tracer kinetic modeling of the 5-HT1A receptor ligand [carbonyl-^{11}C]WAY-100635 for PET. *Neuroimage.* 1998;8:426–440.
14. van der Veldt AA, Hendrikse NH, Harms HJ, et al. Quantitative parametric perfusion images using ^{15}O-labeled water and a clinical PET/CT scanner: test-retest variability in lung cancer. *J Nucl Med.* 2010;51:1684–1690.
15. Yaqub M, Boellaard R, Kropholler MA, Lammertsma AA. Optimization algorithms and weighting factors for analysis of dynamic PET studies. *Phys Med Biol.* 2006;51:4217–4232.
16. Akaike H. A new look at the statistical model identification. *IEEE Trans Automat Contr.* 1974;19:716–723.
17. Larimer BM, Dubois F, Bloch E, et al. Specific ^{18}F-FDHT accumulation in human prostate cancer xenograft murine models is facilitated by prebinding to sex hormone-binding globulin. *J Nucl Med.* 2018;59:1538–1543.
18. Swerdloff RS, Dudley RE, Page ST, Wang C, Salameh WA. Dihydrotestosterone: biochemistry, physiology, and clinical implications of elevated blood levels. *Endocr Rev.* 2017;38:220–254.
19. Selby C. Sex hormone binding globulin: origin, function and clinical significance. *Ann Clin Biochem.* 1990;27:532–541.
20. Kramer GM, Frings V, Hoetjes N, et al. Repeatability of quantitative whole-body ^{18}F-FDG PET/CT uptake measures as function of uptake interval and lesion selection in non-small cell lung cancer patients. *J Nucl Med.* 2016;57:1343–1349.
21. Oprea-Lager DE, Kramer G, van de Ven PM, et al. Repeatability of quantitative ^{18}F-fluoromethylcholine PET/CT studies in prostate cancer. *J Nucl Med.* 2016;57:721–727.
22. Brambilla DJ, Matsumoto AM, Araujo AB, McKinlay JB. The effect of diurnal variation on clinical measurement of serum testosterone and other sex hormone levels in men. *J Clin Endocrinol Metab.* 2009;94:907–913.